Structural Chemistry (2021) 32:539–551
https://doi.org/10.1007/s11224-020-01671-0

ORIGINAL RESEARCH

Crystal structure and vibrational spectra of salts of 1H-pyrazole-1-carboxamidine and its protonation route

Piotr Rejnhardt[1] · Marek Daszkiewicz[1]

Received: 2 October 2020 / Accepted: 27 October 2020 / Published online: 10 November 2020

Abstract

Crystal structures of five salts of 1H-pyrazole-1-carboxamidine, PyCA, with various inorganic acids were determined, (HPyCA)Cl, (HPyCA)Cl·H_2O, (HPyCA)Br, $(HPyCA)_2(I)I_3$, and $(HPyCA)HSO_4$. Theoretical calculations of the protonation route of PyCA showed that the cationic form present in the studied crystals is energetically privileged. Tautomeric equilibrium constants indicated two isomers as the most stable neutral forms. Calculations for two other tautomers failed resulting in pyrazole and carbodiimid tautomer of cyanamide. Such decomposition is important in a view of guanylation reaction. Hydrogen bonding patterns were studied by means of the graph-set approach. Similarities of the patterns in different crystal structures were demonstrated by the algebraic relations between descriptors of the patterns. The strength of hydrogen bonding network in the crystals was assessed analyzing vibrational spectra. The bands were assigned on the basis of theoretical calculations for the complex $[(HPyCA)_2Cl_4]^{2-}$ ion and potential energy distribution analysis. The strength of hydrogen bonds was set in the following ascending series $(HPyCA)_2(I)I_3$ (**4**) < (HPyCA)Br (**3**) < (HPyCA)Cl (**1**) < (HPyCA)Cl·H_2O (**2**) < $(HPyCA)HSO_4$ (**5**).

Keywords Guanylation · Protonation route · Hydrogen bonding · Elementary graph-set descriptor · Vibrational spectroscopy · PED

Introduction

The 1H-pyrazole-1-carboxamidine, hereafter PyCA, has been a next-generation substrate for guanylation of amines after *S*-methylisothiouronium sulfate, cyanamide or 3,5-dimethyl-1-guanylpyrazole nitrate [1]. For instance, it was successfully used in the introduction of guanidinium group as the last step of synthetic procedure of zanamivir, an influenza A and B drug [2], or Boc protected PyCA was a guanylation agent in synthesis of dengue and West Nile virus protease inhibitors [3].

The 1H-pyrazole-1-carboxamidine is commercially available as a hydrochloride and is widely used in organic synthesis for years. It can be synthesized by mixing equimolar amount of pyrazole and cyanamide, and further crystallization from the reaction mixture [1]. This very simple one-step procedure and very simple isolation method of pure compound make the PyCA a low-cost reagent in organic synthesis. The (HPyCA)Cl has very good solubility in water or DMF and is stable even at basic conditions, i.e., 1 M water solution of 1 M Na_2CO_3 [1]. So, it was suggested that the guanylation mechanism proceeds with cationic form of 1H-pyrazole-1-carboxamidine and deprotonated form of respective amine. However, our preliminary search in *Cambridge Structural Database* revealed that crystal structure of PyCA or its salts have not been studied so far [4, 5].

Apart from pyrazole ring, a molecule of PyCA possesses three hydrogen atoms at the carboxyamidine residue forming NH_2 and NH groups. It is worth noticing that a free nitrogen atom of the pyrazole ring may be theoretically faced to the NH_2 or NH groups. Besides, the hydrogen atom of the NH group can be oriented in *syn* or *anti* position. In the first protonation step, the proton can be accepted either to the NH group or to the free nitrogen atom in the pyrazole ring. So, all these facts indicate that a few tautomers of neutral as well as cationic speciation forms of PyCA are expected in the solution. Here, we present theoretical investigation of the route of protonation of PyCA, which has an importance for

Supplementary Information The online version contains supplementary material available at https://doi.org/10.1007/s11224-020-01671-0.

✉ Marek Daszkiewicz
m.daszkiewicz@intibs.pl

[1] Institute of Low Temperature and Structure Research, Polish Academy of Sciences, Okólna str. 2, 50-422 Wrocław, Poland

Table 1 Crystal data and structure refinement for (HPyCA)Cl (**1**), (HPyCA)Cl·H_2O (**2**), (HPyCA)Br (**3**), $(HPyCA)_2(I)I_3$ (**4**), (HPyCA)HSO_4 (**5**)

Chemical formula	$C_4H_7N_4$·Cl	$C_4H_7N_4$·Cl·H_2O	$C_4H_7N_4$·Br	$2(C_4H_7N_4)$·I_3·I	$C_4H_7N_4$·HSO_4
M_r	146.59	164.60	191.05	729.87	208.20
Crystal system, space group	Monoclinic, $P2_1/n$	Triclinic, P–1	Monoclinic, $P2_1/c$	Triclinic, P–1	Monoclinic, $P2_1/c$
a, b, c (Å)	4.8201(3), 14.0874(14), 9.8888(10)	4.8942(5), 9.0867(10), 9.4342(12)	4.8597(2), 9.4774(4), 15.2411(6)	7.3359(3), 10.6942(4), 12.9130(5)	10.6853(7), 9.6487(6), 8.1609(6)
α, β, γ (°)	90, 92.566(6), 90	68.408(11), 87.383(9), 81.492(8)	90, 90.576(4), 90	72.536(3), 75.929(3), 85.996(3)	90, 94.293(6), 90
V (Å^3)	670.80(10)	385.81(8)	701.93(5)	937.35(7)	839.03(10)
Z	4	2	4	2	4
μ (mm^{-1})	0.48	0.44	5.77	6.65	0.38
Crystal size (mm)	0.45 × 0.25 × 0.09	0.63 × 0.20 × 0.08	0.61 × 0.48 × 0.39	0.48 × 0.13 × 0.05	0.42 × 0.35 × 0.08
T_{min}, T_{max}	0.894, 0.972	0.850, 0.969	0.143, 0.247	0.182, 0.767	0.868, 0.971
No. of measured, independent and observed [$I > 2\sigma(I)$] reflections	4156, 1414, 1059	2936, 1621, 1313	6248, 1476, 1218	7975, 3891, 3112	3865, 1850, 1571
R_{int}	0.027	0.022	0.037	0.024	0.017
$(\sin\theta/\lambda)_{max}$ (Å^{-1})	0.633	0.633	0.633	0.633	0.649
$R[F^2 > 2\sigma(F^2)]$, $wR(F^2)$, S	0.043, 0.109, 1.03	0.052, 0.161, 1.10	0.036, 0.094, 1.03	0.033, 0.069, 1.01	0.035, 0.090, 1.07
No. of reflections and parameters	1414, 82	1621, 97	1476, 82	3891, 181	1850, 120
$\Delta\rangle_{max}$, $\Delta\rangle_{min}$ (e Å^{-3})	0.19, −0.22	0.55, −0.28	0.90, −0.53	0.66, −0.82	0.18, −0.37

understanding guanylation reaction. Crystal structures of new PyCA salts with inorganic acids are described. Hydrogen bonding networks are analyzed by topological approach and graph-set descriptors [6, 7]. The compounds are also characterized by infra-red and Raman spectra. The bands are assigned with the help of theoretical simulations and potential energy distribution (PED) analysis.

Materials and methods

Synthesis

The starting compounds, (HPyCA)Cl (ArkPharm Inc., 97+ %), hydrofluoric acid (Aldrich, ≥ 57 wt % in H_2O), hydrobromic acid (Aldrich, ≥ 48 wt % in H_2O), hydroiodic acid (Aldrich, 57 wt % in H_2O, 99.95 %, no stabilizer), and sulfuric acid (Aldrich, 95.0–98.0 wt % in H_2O, 99.95 %) were used as supplied. The (HPyCA)Cl was re-crystallized from 3 ml of methanol. In each synthesis, the (HPyCA)Cl (1 mmol, 0.1466 g) was dissolved in 3 ml of methanol and then respective acid was added: 1 ml HF, 1.5 ml HBr, 1 m HI, and 1 ml H_2SO_4. The crystals of (HPyCA)Br (**3**) and (HPyCA)HSO_4 (**5**) were obtained after 1 to 5 days by slow evaporation of the mixture in air at room temperature. The crystals of $(HPyCA)_2(I)I_3$ (**4**) were formed after 2 months, whereas (HPyCA)Cl·H_2O (**2**) was obtained instead of fluoride salt.

Single crystal X-ray diffraction studies

X-ray diffraction data were collected on an Oxford Diffraction four-circle single crystal diffractometer equipped with a CCD detector using graphite-monochromatized MoK_α radiation (λ = 0.71073 Å). The raw data were treated with the CrysAlis Data Reduction Program (version 1.171.38.43). The intensities of the reflection were corrected for Lorentz and polarization effects. The crystal structures were solved by direct methods [8] and refined by full-matrix least-squares method using SHELXL-2017 program [9]. Non-hydrogen atoms were refined using anisotropic displacement parameters. All H-atoms were visible on the Fourier difference maps, but placed by geometry and allowed to refine "riding on" the parent atom (with U_{iso} = 1.2 U_{eq} for sp^2-carbon atoms, and U_{iso} = 1.5 U_{eq} for other atoms). Visualizations of the structure were made using Diamond 3.2 k [10]. Low temperature X-ray diffraction experiments were carried out using Oxford Cryosystems device in the range of 295–100 K with temperature step ΔT = 10 K, but no phase transition was observed for all the crystals. Crystal data and refinement details are presented in Table 1.

Spectroscopic measurements

Room temperature FT-IR spectra in the 4000–400 cm^{-1} range were measured on the Bruker IFS-88 spectrometer with 2 cm^{-1} resolution. Nujol and fluorolube mull techniques have been used in the measurements. Nd:YAG laser (1064 nm) was used to collect room temperature FT-Raman spectra, which were

Table 2 Total energy (Hartree), zero-point energy plus thermal corrections ($E_{thermal}$, kcal/mol) and entropy (cal/molK) for the neutral and protonated forms of 1H-pyrazole-1-carboxamidine

	E_{total}	$E_{thermal}$	Entropy
Carbodiimid	− 148.8320638	22.683	58.442
Pyrazole	− 226.2718376	46.971	65.122
PyCa			
23a4a	− 375.0939469	72.286	80.798
3a4ab	− 375.1223137	71.69	77.644
3b4ab	− 375.1341123	72.011	77.215
3ab4b	− 375.1397131	72.518	80.706
3ab4a	− 375.1428629	72.621	79.85
$HPyCA^+$			
23ab4b	− 375.4810472	79.832	79.154
23b4ab	− 375.4842483	79.776	78.842
23ab4a	− 375.4904709	79.994	79.308
23a4ab	− 375.5049725	80.711	81.606
3ab4ab	− 375.5242936	81.533	86.952
H_2PyCa^{2+}			
23ab4ab	− 375.7032165	88.848	82.115

Table 3 Gibbs free energy (kJ/mol) and tautomer equilibrium constant (K_T) for tautomeric equilibria of the neutral and protonated forms of 1H-pyrazole-1-carboxamidine

	ΔG	K_T
Carbodiimid + pyrazol = 3ab4a	− 45.26	
Carbodiimid + pyrazol = 3ab4b	− 38.49	
Carbodiimid + pyrazol = 3b4ab	− 21.55	
Carbodiimid + pyrazol = 3a4ab	7.55	
Carbodiimid + pyrazol = 23a4a	80.58	
3ab4b = 3ab4a	− 6.77	$1.54 \cdot 10^1$
3b4ab = 3ab4a	− 23.71	$1.43 \cdot 10^4$
3a4ab = 3ab4a	− 52.81	$1.79 \cdot 10^9$
23a4a = 3ab4a	− 125.85	$1.12 \cdot 10^{22}$
H^+ + 3ab4a = $3ab4ab^+$	− 979.21	
H^+ + 3ab4a = $23a4ab^+$	− 925.26	
H^+ + 3ab4a = $23ab4a^+$	− 887.32	
H^+ + 3ab4a = $23b4ab^+$	− 871.31	
H^+ + 3ab4a = $23ab4b^+$	− 863.06	
$23a4ab^+$ = $3ab4ab^+$	− 53.96	$2.84 \cdot 10^9$
$23ab4a^+$ = $3ab4ab^+$	− 91.90	$1.26 \cdot 10^{16}$
$23b4ab^+$ = $3ab4ab^+$	− 107.90	$8.03 \cdot 10^{18}$
$23ab4b^+$ = $3ab4ab^+$	− 116.15	$2.24 \cdot 10^{20}$
H^+ + $3ab4ab^+$ = $23ab4ab^{2+}$	− 439.32	

Table 4 Theoretical frequencies for the $([(HPyCA)_2Cl_4]^{2-}$ ion scaled by $\nu_{sc} = 0.9614 \cdot \nu_{calc} + 17.8$ equation (ν_{sc}), mode symmetry (S), experimental frequencies taken from infrared ($\nu_{exp,\ IR}$) and Raman ($\nu_{exp,\ R}$) spectra for (HPyCA)Cl (**1**) compound, PED (%) and assignment of the experimental bands. Frequencies in cm^{-1}

ν_{sc}	S	$\nu_{exp,\ IR}$	$\nu_{exp,\ R}$	PED	Assignment
3443	A_g			s1(96)	νNH(3b)
3432	A_u	3379		s2(97)	νNH(3b)
		3227			
3156	A_g		3134	s3(96)	νCH
3156	A_u	3128		s4(96)	νCH
3116	A_u	3100		s5(93)	νCH
3116	A_g		3102	s6(95)	νCH
3105	A_u	3321		s7(93)	ν_sNH_2(3a + 4a)
3103	A_g			s8(95)	ν_sNH_2(3a + 4a)
3026	A_g		3024	s9(85)	$\nu_{as}NH_2$(3a + 4a)
3025	A_u	3026		s10(87)	$\nu_{as}NH_2$(3a + 4a)
2998	A_g		3064	s11(91)	νCH
2997	A_u			s12(92)	νCH
2825	A_g			s13(87)	νNH(4b)
2821	A_u	2753		s14(88)	νNH(4b)
		2346			
		1806			
		1768			
1705	A_g		1634	s15(62) s23(13) s68(10)	$\nu_{as}CN_{(gua)}$
1703	A_u	1702		s16(62) s24(14) s69(10)	$\nu_{as}CN_{(gua)}$
1613	A_u	1669		s17(88)	δ_sNH_2
1611	A_g		1570	s18(80)	δ_sNH_2
1545	A_u	1554		s19(35) s24(12) s21(10)	$\nu CN_{(gua)}$
1537	A_g		1538	s20(53) s39(12)	νCC + νCN
1529	A_u	1537		s21(51)	νCC + νCN
1523	A_g			s22(44) s36(13) s38(12)	$\nu CN_{(gua)}$
1506	A_g			s23(64) s22(13) s15(10)	δ_sNH_2
1504	A_u			s24(58)s16(11)	δ_sNH_2
1408	A_g		1408	s31(23) s25(17) s28(12) s41(10)	νCN
1408	A_u	1412		s26(19) s33(14) s40(11) s32(10) s62(10)	νCC + νCN
1401	A_u	1398		s27(48) s26(13)	ρCC
1400	A_g		1394	s28(39) s39(37)	νCC
1309	A_u	1309		s29(57)	νCN
1309	A_g		1311	s30(51)	νCN
1231	A_g		1233	s31(54) s25(13)	νCN + νCC
1230	A_u	1231		s32(57) s27(11) s33(10)	νCN + νCC
1221	A_u	1222		s33(30) s21(13) s44(10)	δCH
1218	A_g		1217	s34(36) s25(34) s36(10)	νNN + δCH
1140	A_u			s35(50)	ρNH_2
1139	A_g		1128	s36(34) s20(10)	ρNH_2
1127	A_u	1127		s37(57) s40(10)	ρNH_2
1117	A_g		1089	s38(61) s22(14)	ρNH_2
1091	A_g		1080	s39(15) s36(13) s22(12) s34(11) s20(10)	δCH + ρNH_2
1090	A_u	1099		s40(23) s35(14) s21(10) s27(10)	δCH + ρNH_2
1043	A_g		1046	s41(52) s28(22)	δCH
1042	A_u	1055		s42(51) s26(31)	δCH
945	A_g			s43(52) s41(19)	δCH + δCNN
943	A_u			s44(54) s71(11) s42(10)	δCH + δCNN
940	A_u			s45(81)	γCH
940	A_g		942	s46(84)	γCH
927	A_u	947		s47(88)	Ring breathing
		929			
927	A_g		909	s48(82)	Ring breathing
892	A_g		869	s49(87)	γCH
892	A_u	911		s50(89)	γCH
859	A_u	886		s51(52)	τNH_2
855	A_g			s52(80)	τNH_2
826	A_u	845		s53(57) s51(22)	ωNH_2
824	A_g			s54(78)	ωNH_2
781	A_u	781		s55(88)	γCH
780	A_g		782	s56(88)	γCH
726	A_u	736		s57(65) s53(16)	$\tau NH_2 + \gamma NH_2$
724	A_g			s58(65)	$\tau NH_2 + \gamma NH_2$

Table 4 (continued)

ν_{sc}	S	$\nu_{exp,\ IR}$	$\nu_{exp,\ R}$	PED	Assignment
706	A_g			s59(77)	$\gamma CN_{(gua)}$
705	A_u			s60(75)	γNH_2
697	A_g		691	s61(61)	$\nu_s CN_{(gua)}$
694	A_u	685		s62(56) s40(25)	$\nu_s CN_{(gua)}$
650	A_g		641	s63(86)	γCCN
647	A_u	655		s64(80)	γCCN
600	A_g			s65(86)	γCCN
600	A_u	635		s66(84)	γCCN
572	A_u	574		s67(68)	$\gamma CN_{(gua)}$
536	A_g		575	s68(71)	$\nu CN_{(gua)}$
533	A_u	538		s69(69)	$\nu CN_{(gua)}$
507	A_g			s70(82)	γNH_2
475	A_u	469		s71(53) s19(16) s79(15)	$\nu CN_{(gua)}$
474	A_g		474	s72(59) s61(13)	$\nu CN_{(gua)}$
			464		
299	A_u			s73(70)	$\rho CN_{(gua)}$
295	A_g		276	s74(59) s85(11)	$\rho CN_{(gua)}$
192	A_g			s75(75)	$\gamma CN_{(gua)}$
191	A_u			s76(83)	$\gamma CN_{(gua)}$
190	A_g			s77(76)	Lattice
189	A_u			s78(82)	Lattice
184	A_u			s79(73)	Lattice
182	A_g			s80(75)	Lattice
132	A_u			s81(84)	Lattice
129	A_g			s82(72)	Lattice
123	A_u			s83(85)	$\tau CN_{(gua)}$
113	A_g			s84(80)	$\tau CN_{(gua)}$
95	A_g			s85(48) s26(13)	Lattice
92	A_u			s86(74)	Lattice
87	A_g			s87(76)	Lattice
87	A_u			s88(74)	Lattice
77	A_g			s89(63) s92(14)	Lattice
73	A_g			s90(66)	Lattice
67	A_u			s91(66) s51(14)	Lattice
48	A_g			s92(68) s89(13)	Lattice
44	A_g			s93(63)	Lattice
42	A_u			s94(65) s90(13)	Lattice
39	A_u			s95(88)	Lattice
8	A_u			s96(71)	Lattice

measured in the 3600–80 cm^{-1} range with 2 cm^{-1} resolution using Bruker IFS-88 instrument with FRA-106 attachment. Raman spectrum for (HPyCA)(I)I_3 was recorded using a Renishaw InVia Raman spectrometer equipped with a confocal DM 2500 Leica optical microscope.

Computational details

All the computations were performed with the Gaussian 16 program [11]. The calculations were carried out using density-functional theory (DFT) and hybrid Becke's three-parameter and the Lee–Yang–Parr correlation functionals (B3LYP) [12–15] with Grimme's correction for dispersion with Becke–Johnson damping [16]. The 6-311G(d,p) basis set was used, because it gives satisfactory results for vibrational and thermochemical data with respect to the computational costs [17]. For all the neutral and protonated forms of the PyCA, the minima were found for the singlet electronic state. Calculated total energy, zero-point energy (ZPE) plus thermal corrections and entropy are listed in Table 2, whereas Gibbs free energy and tautomer equilibrium constant for tautomeric equilibria of the neutral and protonated forms of 1H-pyrazole-1-carboxamidine are shown in Table 3.

Vibrational frequencies were calculated for protonated form of 1H-Pyrazole-1-carboxamidine, i.e., $HPyCA^+$ ion. Since the $HPyCA^+$ ion is involved in hydrogen bonding network in the studied crystal structures, the calculations were also carried out for the centrosymmetric $[(HPyCA)_2Cl_4]^{2-}$ ionic system present in the crystal structure of (HPyCA)Cl (**1**). The positions of all the atoms were taken from crystallographic data, and a constrain with C_i point group symmetry for geometry parameters was applied. Additionally, positions of four chloride anions were frozen in order to prevent the ions from escaping to infinity. Frequency of normal modes was

Table 5 Experimental frequencies taken from infrared ($\nu_{exp,\ IR}$) and Raman ($\nu_{exp,\ R}$) spectra for (HPyCA)Cl·H_2O (**2**), (HPyCA)Br (**3**), $(HPyCA)_2(I)I_3$ (**4**), $(HPyCA)HSO_4$ (**5**) and assignment of the experimental bands. Frequencies in cm^{-1}

$\nu_{exp,\ IR}$ (2)	$\nu_{exp,\ R}$ (2)	$\nu_{exp,\ IR}$ (3)	$\nu_{exp,\ R}$ (3)	$\nu_{exp,\ R}$ (4)	$\nu_{exp,\ IR}$ (5)	$\nu_{exp,\ R}$ (5)	Assignment
				3346			νNH
3380		3376			3363		νNH
				3207		3151	
3235							
	3132		3129	3132		3135	νCH
3128		3125			3139		νCH
				3052			
3101		3099					νCH
	3123		3109	3111		3121	νCH
3317		3316					ν_sNH_2
				3275			ν_sNH_2
				3207			$\nu_{as}NH_2$
3023							$\nu_{as}NH_2$
	3063		3060	3083			νCH
2753		2778					νNH
2646		2644			2562		
					2453		
2342		2330			2326		
2249							
2194					2194		
1843		1844			1836		
1805		1801					
	1633		1635	1619		1662	$\nu_{as}CN_{(gua)}$
			1625				
1700		1699			1707		$\nu_{as}CN_{(gua)}$
1669		1660			1647		δ_sNH_2
1624							
	1568		1567	1556		1572	δ_sNH_2
1554		1558			1568		$\nu CN_{(gua)}$
	1538		1549	1541			νCC + νCN
1537		1538			1534		νCC + νCN
			1532	1529		1537	$\nu CN_{(gua)}$
	1407		1408	1416		1407	νCN
1409		1413			1441		νCC + νCN
1397		1395			1391		ρCC
	1395			1391		1392	νCC
1309		1309			1306		νCN
	1310		1307	1309		1308	νCN
	1234		1227	1223		1229	νCN + νCC
1221		1220			1216		δCH
					1168		
	1216		1214	1213		1206	νNN + δCH
	1129		1112	1105		1124	ρNH_2
1128		1120			1130		ρNH_2
	1088						ρNH_2
	1081		1080	1084		1081	δCH + ρNH_2
1099		1097			1081		δCH + ρNH_2
	1047		1045	1057		1045	δCH
				1041		1023	
1055		1050			1068		δCH
					1026		
	941		941	942		936	γCH
947		944			937		ring breathing
927		928			919		
	910		909	909		910	ring breathing
	868		873	863		878	γCH
				837			
911		910			911		γCH
885		884			880		τNH_2
847		837			850		ωNH_2
784		774			783		γCH
					758		
			785	758			γCH
735		730			723		$\tau NH_2 + \gamma NH_2$

Table 5 (continued)

$\nu_{exp,\ IR}$ (2)	$\nu_{exp,\ R}$ (2)	$\nu_{exp,\ IR}$ (3)	$\nu_{exp,\ R}$ (3)	$\nu_{exp,\ R}$ (4)	$\nu_{exp,\ IR}$ (5)	$\nu_{exp,\ R}$ (5)	Assignment
		698					γNH_2
	691		688	670		691	$\nu_s CN_{(gua)}$
			670				
685		681			676		$\nu_s CN_{(gua)}$
	641		648			638	γCCN
659		644					γCCN
			630			608	γCCN
634		633			634		γCCN
					597		
					585		
					571		
574		558					$\gamma CN_{(gua)}$
	574		582	579		573	$\nu CN_{(gua)}$
537		536			530		$\nu CN_{(gua)}$
					513		
			531	528		513	γNH_2
468		460			457		$\nu CN_{(gua)}$
					433		
	473		453	447		452	$\nu CN_{(gua)}$
						431	
						417	
	464						
			275	334			$\rho CN_{(gua)}$
				221		222	$\gamma CN_{(gua)}$

scaled using scaling equation $\nu_{sc} = 0.9614 \cdot \nu_{calc} + 17.8$ [17]. Juxtaposition of experimental and calculated frequencies for $HPyCA^+$ ion and $[(HPyCA)_2Cl_4]^{2-}$ ionic system and assignment of the bands are presented in the Tables 4 and 5, and in Supplementary Information.

Results and discussion

Protonation of 1H-pyrazole-1-carboxamidine

Theoretically, the neutral molecule of 1H-pyrazole-1-carboxamidine has as many as eight tautomers (Scheme 1). In this work, the tautomers are named after the labels of hydrogen atoms connected to the nitrogen atoms. This labeling scheme is inherited from crystallographic data (Fig. 1). For instance, the 3ab4a abbreviation means that two hydrogen atoms are bound to the N3 atom in *a* and *b* positions, one H-atom is connected to the N4 atom in *a* position, but aromatic N2 atom is free, because its label does not occur in the abbreviation. A protonation route for the PyCA is presented in Scheme 1.

Table 2 shows that the most stable geometry is observed for 3ab4a form. However, calculations for the 23b4a, 23b4b, and 23a4b isomers failed revealing their instability. In the case of 23a4b isomer, a hydrogen atom bound to pyrazole N2 atom moved to the 3b position during geometry optimization. As a result, another isomer was formed, 3ab4b, which is the second most stable tautomer of PyCA neutral molecule. Surprisingly, there is one stable tautomer where the hydrogen atom is attached to the N2 atom, 23a4a, although it is featured by the highest energy (Table 2). The 23a4a form is probably a zwitterion consisting of a positively charged pyrazole and a negatively charged carboxamidine residue. It is worth noting that possible hopping of the hydrogen atom from N2 atom to 3b position in 23a4a results in the most stable 3ab4a form. Such proton transfer proceeds by analogy to the transformation between 23a4b and 3ab4b isomers, and it is very likely due to low ΔG for tautomerization to the energetically privileged 3ab4a form.

The calculations also revealed decomposition of both 23b4a and 23b4b isomers into pyrazole and cyanamide (its carbodiimid tautomer) during optimization of their structure. These results indicate strongly unfavorable binding of two hydrogen atoms to the N2 atom and at 3b site. Therefore, free energy for formation of PyCA from pyrazole and carbodiimid was calculated for five stable species. The only three isomers are featured by negative ΔG and the value for 23a4a relatively highly positive (Table 3). The tautomeric equilibrium constants clearly reveal that the main neutral form of PyCA is 3ab4a which stays in quite relevant equilibrium with 3ab4b tautomer.

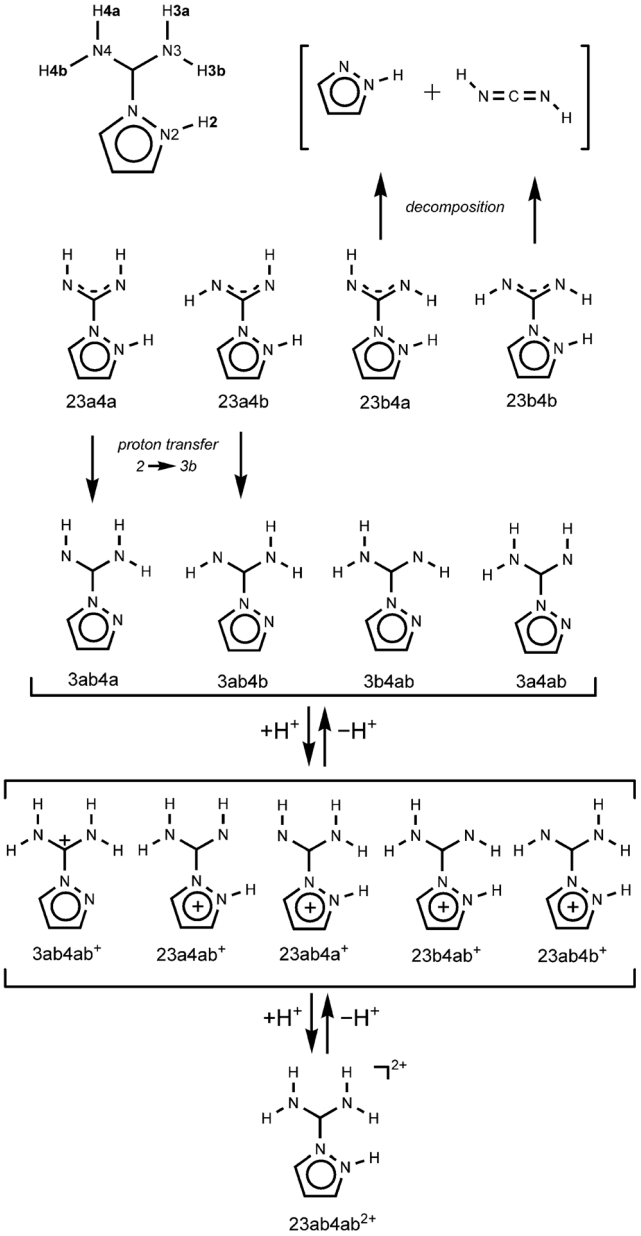

Scheme 1 Protonation route for 1H-pyrazole-1-carboxamidine

The first protonation step theoretically gives five products. All these reactions are featured by large negative free energy. However, they differ from each other as much as one cationic form $3ab4ab^+$ is a dominant product at the first protonation step. The tautomeric equilibrium constants for the cations indicate that approximately only one molecule of the second energetically stable $23a4ab^+$ ion may appear over a billion $3ab4ab^+$ ions. Besides, a molecule of the highest unfavorable $23ab4b^+$ tautomer can be found in the surroundings of 1 mmol of $3ab4ab^+$ ions. So, the latter is reasonably expected in solution as well as in a crystalline product obtained from acidic conditions.

The protonation route of PyCA eventually ends at the second stage leading to the formation of the $23ab4ab^{2+}$ ion. Here,

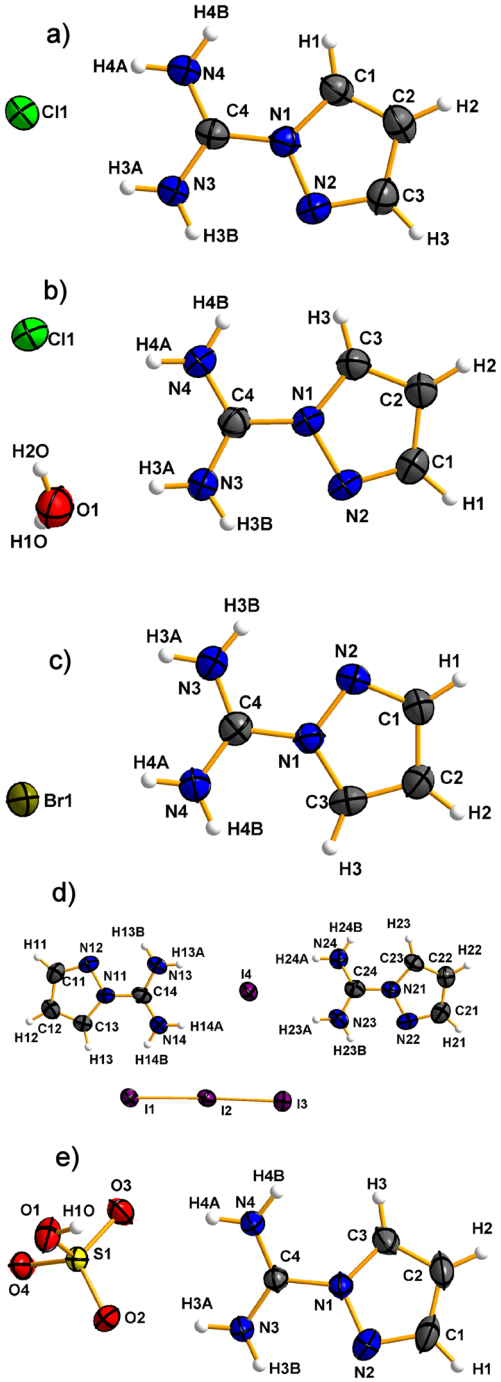

Fig. 1 Molecular structure and labeling scheme for **a** (HPyCA)Cl – **1**, **b** (HPyCA)Cl·H_2O – **2**, **c** (HPyCA)Br – **3**, **d** $(HPyCA)_2(I)I_3$ – **4**, and **e** $(HPyCA)HSO_4$ – **5**

all the proton acceptors are occupied. Since the protonation free energy is negative, formation of the $23ab4ab^{2+}$ ion bearing compound is also probable. However, it is worth noticing that the value of ΔG is twice lower than in the first protonation stage. So, any effort to obtain a crystalline product containing $23ab4ab^{2+}$ cation requires a strongly acidic condition.

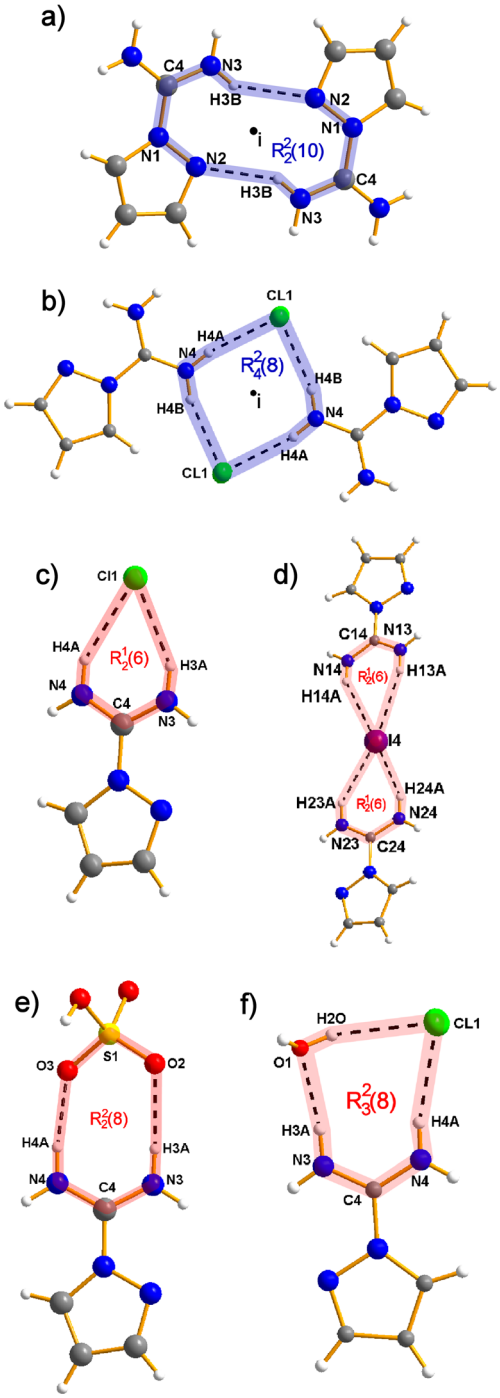

Fig. 2 **a**–**f** Ring patterns formed by the $HPyCA^+$ ion in the studied crystals

Role of pyrazole and carboxamidine residue in formation of hydrogen bonding patterns

All the presented salts of 1H-pyrazole-1-carboxamidine crystallize in centrosymmetric space groups of monoclinic or triclinic symmetry (Table 1). The common feature of the studied compounds is the presence of the same cationic form of $HPyCA^+$ ion, labeled as 3ab4ab$^+$ in the former theoretical section, which is the most energetically privileged tautomer among all the $HPyCA^+$ cations. Since the N2 atom of pyrazole ring is not protonated, it may play an acceptor role in a hydrogen bonding network. In the crystal structures of (HPyCA)Cl (**1**), (HPyCA)Cl·H_2O (**2**), and (HPyCA)Br (**3**), two $HPyCA^+$ are complementary arranged around the inversion center. The ions are connected to each other by two N3–H3B···N2 hydrogen bonds forming a ring pattern, $R^2_2(10)$ (Fig. 2a). Interestingly, it is the only characteristic motif created by the N2 atom in the studied crystal structures. Two NH_2 groups of the carboxamidine residue and two anions create another ring pattern $R^2_4(8)$, which is composed similarly to the $R^2_2(10)$ ring around the inversion center (Fig. 2b). This pattern occurs in the crystal structure of bisulfate and two chloride salts.

Figure 2c–f shows also small rings arranged in an ascending order $R^1_2(6) < R^2_2(8) < R^2_3(8)$. Formation of these patterns can be expressed by the sum of the elementary graph-set descriptors, $E^a_d(n)$, which were originally invented for description of atomic pathways in each independent molecule [6, 7]. A juxtaposition of the molecules and formation of hydrogen bonding patterns are represented by the algebraic equation of elementary graph-set descriptors. Thus, the aforementioned rings are created as follows:

$$E^0_2(5)_{HNCNH} + E^1_0(1)_{Cl/I} = R^1_2(6)\ \text{(HPyCA)Cl (1) and (HPyCA)}_2\text{(I)I}_3\ \text{(4)}$$

$$E^0_2(5)_{HNCNH} + E^2_0(3)_{OSO} = R^2_2(8)\ \text{(HPyCA)HSO}_4\ \text{(5)}$$

$$E^0_2(5)_{HNCNH} + E^1_0(1)_{Cl} + E^1_1(2)_{HO} = R^2_3(8)\ \text{(HPyCA)Cl} \cdot H_2O\ \text{(2)}$$

The first one occurs in the chloride salt (**1**) and bases on the bifurcated hydrogen bonding interaction of one chloride anion. The same two rings are found in $(HPyCA)_2(I)I_3$ (**4**) and they are arranged in the pseudo centrosymmetric binary system. So, one iodide anion takes part in as many as four hydrogen bonds and such surrounding of the anion is not present in the other studied crystal structures. In the bisulfate salt (**5**), the ring pattern is naturally enlarged due to two oxygen atoms are involved in hydrogen bonding network. Therefore, the simplest ring $R^1_2(6)$ is expanded by the S–O two-atomic pathway, which can be expressed by the elementary graph-set $E^1_0(2)_{SO}$. Using algebraic approach, a relation between two patterns found in chloride and bisulfate is written as $R^1_2(6) + E^1_0(2) = R^2_2(8)$. Similarly, the ring $R^2_3(8)$ present in (HPyCA)Cl·H_2O (**2**) results from expansion of the simplest $R^1_2(6)$ pattern by the O–H pathway $R^1_2(6) + E^1_1(2) = R^2_3(8)$.

Apart from the rings, the chain patterns have got high importance in a view of propagation of the crystal structure and of the crystal growth. In $(HPyCA)HSO_4$ (**5**), (HPyCA)Cl·H_2O (**2**), and (HPyCA)Cl (**1**), very short chain patterns containing only four atoms are found, $C^1_1(4)$ or $C^1_2(4)$. The former is

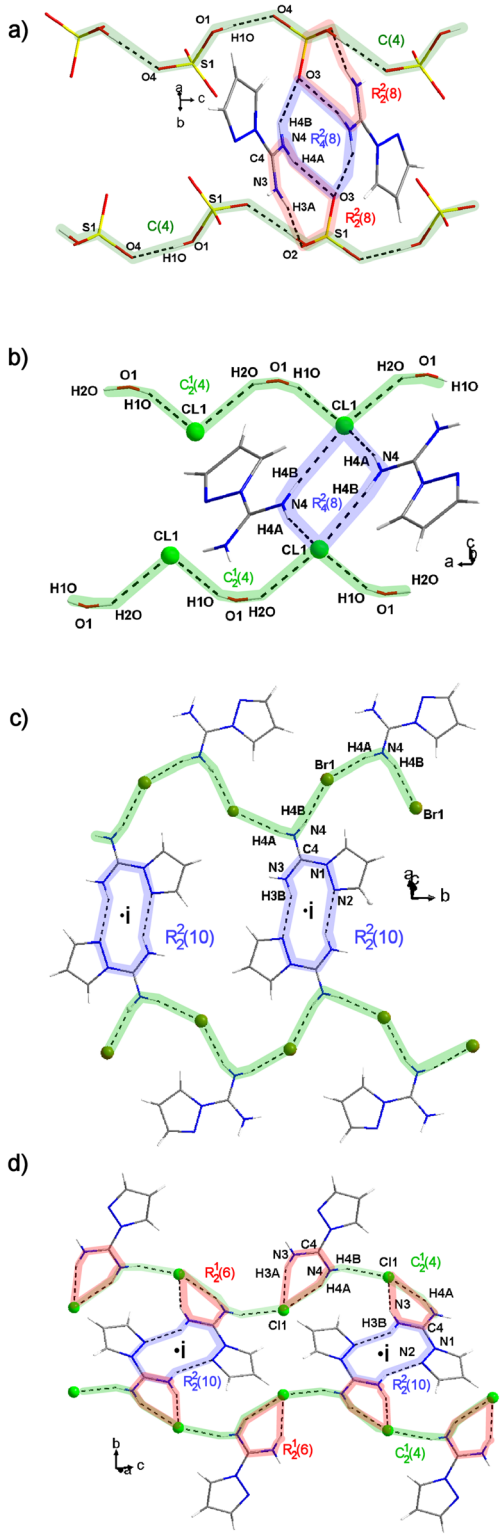

Fig. 3 Hydrogen bonding network in **a** $(HPyCA)HSO_4$ – **5**, **b** $(HPyCA)Cl{\cdot}H_2O$ – **2**, **c** (HPyCA)Br – **3**, and **d** (HPyCA)Cl – **1**

created by the only one symmetry independent O1–H1O···O4 hydrogen bond and exists in the crystal structure of $(HPyCA)HSO_4$ (**5**) (Fig. 3a). The latter $C^1_2(4)$ chain is observed in $(HPyCA)Cl{\cdot}H_2O$ (**2**) and it runs through the Cl^- anions and water molecules. In the case of (HPyCA)Br (**3**) and (HPyCA)Cl (**1**), the $C^1_2(4)$ chain is constructed by the NH_2 group and anions. So, the organic cations are involved in stabilization of the hydrogen bonding network in the crystal structure of bromide and chloride salts, but interestingly the $HPyCA^+$ ions are completely omitted in those short chains in bisulfate and hydrated chloride salts. Such architecture of the network is probably connected to the high tendency of the bisulfate anions to associate with each other, as a data mining of *Cambridge Structural Database* reveals a lot of crystal structures containing the $(HSO_4^-)_n$ chains [4, 5]. A branched molecular structure of the HSO_4^- ion may also be important in this question.

Figure 3 shows that the chain patterns are connected to each other by the $HPyCA^+$ associated in dimers forming aforementioned $R^2_2(10)$ or $R^2_4(8)$ rings. So, one can infer that the rings play a supporting role in stabilization of the crystal structures. However, their role cannot be regarded as secondary, as creation of the dimers allows crystal growth along orthogonal direction to the chains.

Vibrational characteristics

Geometry data taken from crystal structure analysis show weak nature of N/O–H···donor hydrogen bonds in the studied compounds except one O–H···O interaction. The shortest donor···acceptor distance is observed for the O–H···O hydrogen bond, 2.5969(19) Å (Table S1), formed by the adjacent bisulfate anions in $(HPyCA)HSO_4$ (**5**). According to earlier Novak's work, the band associated with the stretching vibration of hydroxyl group νOH is seen at 2453 cm^{-1} [18]. This value correlates very well with a dependence of OH stretching frequency on O···O distance and indicates medium-strong feature of O–H···O hydrogen bond in the $(HPyCA)HSO_4$ crystal. A medium hydrogen bond of the N–H···O type is created in $(HPyCA)Cl{\cdot}H_2O$ (**2**). Since the N···O distance is 2.800(3) Å, the νNH band is observed in higher frequency region than νOH in the bisulfate salt, 3136 cm^{-1} (Fig. 4). Geometry data for the other N–H···donor hydrogen bonds indicate their weak nature, and therefore, the respective νNH bands are expected near the νCH ones. So, theoretical calculations have been carried out for the $HPyCA^+$ ion and potential energy distribution analysis was performed (Table S2). However, such kind of calculations can provide artificial results; theoretical frequencies of normal modes were also determined for the complex $[(HPyCA)_2Cl_4]^{2-}$ ionic system with C_i point group symmetry constrain for geometry parameters. Generally, Table 4 shows good agreement of the theoretical and experimental frequencies and PED analysis reveals a character of each mode.

According to the crystallographic data, the $HPyCA^+$ ions are arranged in pairs and connected to each other by two relatively long N3–H3B···N2 hydrogen bonds, 3.028(3) Å.

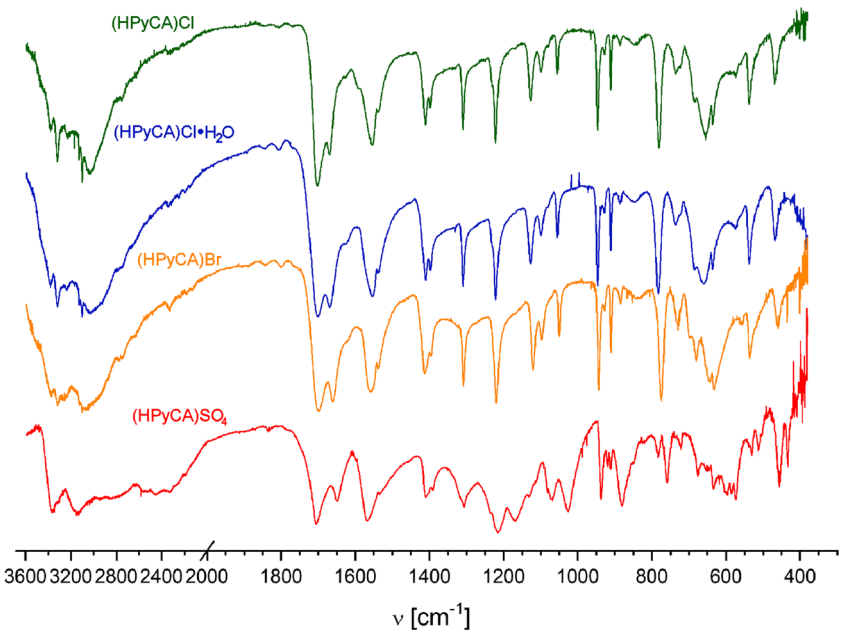

Fig. 4 A juxtaposition of FT-IR spectra for the studied compounds

Although it is the shortest hydrogen bonding interaction in (HPyCA)Cl (**1**), the N–H···N angle is significantly lower than 180 deg indicating very low strength in this intermolecular interaction. Calculations of theoretical frequencies for the $[(HPyCA)_2Cl_4]^{2-}$ anions suggest that the N–H···N hydrogen bond is the weakest one in the crystal structure of (HPyCA)Cl (**1**). Both N3–H3A···Cl1 and N4–H4A···Cl1 have similar geometry, albeit longer N···Cl distance is observed than for N3···N1, which is probably connected to a different radius for nitrogen atom and chloride anion. Those two N–H···Cl hydrogen bonds are expectedly coupled resulting in the symmetric and antisymmetric νNH_2(3a+4b) modes. Accordingly, two well-shaped bands seen in the infrared spectrum at 3321 and 3030 cm^{-1} are assigned. Interestingly, the Raman component of the latter band is probably observed at 3024 cm^{-1}. Calculations also indicate that the strongest hydrogen bond in the (HPyCA)Cl (**1**) is N4–H4B···Cl1, which correlates well with geometry parameters for hydrogen bonds. This interaction is characterized by shortest N···Cl distance and the N–H···Cl angle is the most obtuse. Therefore, the medium band at 2754 cm^{-1} is attributed to the νNH(4b) vibration.

Although (HPyCA)Br (**3**) and (HPyCA)Cl (**1**) crystallize in a different setting of space group no. 14, $P2_1/c$, their hydrogen bonding networks are very similar. Also, the analysis of hydrogen bonding patterns for both (HPyCA)Cl·H_2O (**2**) and (HPyCA)HSO_4 (**5**) in comparison to the chloride salt (**1**) revealed analogies in creation of the chain and ring patterns by the carboxyamidine group. Such a coincidence makes the interpretation of the vibrational spectra much easier. This task is expectedly not to be sophisticated also for $(HPyCA)_2(I)I_3$ (**4**), as the $HPyCA^+$ ion is engaged in weak hydrogen bonds. Therefore, the band assignment is done for the compounds **2-5** on the basis of the results for (HPyCA)Cl (**1**).

A series of relatively broad bands are observed in the infrared spectra in the range of 2000–3600 cm^{-1}. They lie at a little bit higher frequency region in the spectrum of the bromide salt suggesting weaker nature hydrogen bonding network in (HPyCA)Br (**3**). Although one may expect lower strength of intermolecular interactions for $(HPyCA)_2(I)I_3$ (**4**) according to well-known tendency among the halides, the aforementioned νNH bands for **4** appear at approximately the same position as for bromide. Such somewhat unusual result can be associated with two speciation forms of iodide or a multitude of intermolecular interactions (Table S1). In the case of (HPyCA)Cl·H_2O (**2**), both infra-red and Raman spectra have got almost the same shape as (HPyCA)Cl (**1**). However, a few bands covered in the νNH/νOH region result in noticeably broader absorption, especially in the lower frequency part. Taking into account geometry parameters for the N3–H3A···O1 hydrogen bond (Table S1), the maximum of the νOH band is expected below 3000 cm^{-1}. So, the strength of hydrogen bonding network in the hydrated chloride salt appears to be higher than anhydrous chloride.

Apart from stretching modes, several bands associated with the bending vibration of the NH_2 groups are seen in the spectra. The bands attributed to the in-plane bending modes, δNH_2, occur near the νCN bands at 1669 and 1537 cm^{-1} in the infrared spectrum of (HPyCA)Cl (**1**), whereas rocking vibrations are observed at 1127 and 1099 cm^{-1}. The position of these bands does not differ so much for the other studied salts of PyCA. So, a strength of hydrogen bonds can be assessed on the basis of the stretching vibrations in the following ascending series: $(HPyCA)_2(I)I_3$ (**4**) < (HPyCA)Br (**3**) < (HPyCA)Cl (**1**) < (HPyCA)Cl·H_2O (**2**) < (HPyCA)HSO_4 (**5**).

Among all the studied compounds, the internal vibrations of the anion can be observed in the $(HPyCA)_2(I)I_3$ (**4**) and

(HPyCA)HSO_4 (**5**). The fundamental vibration for the I_3^- is observed as the most intense band at the low frequency region in the Raman spectrum of **4**. The maximum lies at 110 cm^{-1} and the first and the second overtones are seen at 221 and 334 cm^{-1}. In the case of the bisulfate anion, its ν_3 stretching vibration of F_2 symmetry in tetrahedral SO_4^{2-} anion splits into two components, 1068 and 1026 cm^{-1}, due to lowering of symmetry from $T_d(SO_4^{2-})$ to $C_{3v}(HSO_4^-)$. Also, the ν_1 mode is associated to the stretching vibration of the S–OH bond. The Raman components for both ν_3 and ν_1 modes are observed at 1023 and 878 cm^{-1}. Among the bending modes ν_4 and ν_2, the one maximum at 433 cm^{-1} in the infra-red spectrum can be tentatively assigned to the ν_4 vibration, whereas the Raman spectrum reveals its two-component feature, 431 and 417 cm^{-1}.

Conclusions

The (HPyCA)Cl (**1**) was used to obtain four new salts of 1H-pyrazole-1-carboxamidine with various inorganic acids. The simplicity of synthetic procedure of presented compounds can be optionally used in organic synthesis wherever other salt than commercially available (HPyCA)Cl (**1**) is required. Since the literature data as well as *Cambridge Structural Database* do not contain any structural data about the salts of PyCA, five crystal structures were determined by means of single-crystal X-ray diffraction and presented here. The topological analysis with algebraic approach on the graph-set descriptors of hydrogen bonding patterns showed similarities in formation of particular patterns regardless of the counterion present in the structure. This fact was also confirmed by vibrational spectroscopy, where some differences in the infra-red spectra were observed in the high frequency region for νNH modes. In all the studied compounds, the $HPyCA^+$ possesses protonated carboxamidine group, whereas the nitrogen atom of pyrazole ring is deprotonated. Theoretical calculations on the protonation route of PyCA revealed that aforementioned speciation cationic form of 1H-pyrazole-1-carboxamidine is the only favored one. Besides, these calculations showed two relatively numerous stable neutral forms and also two other tautomers that are unstable. The molecules decomposed into pyrazole and carbodiimid tautomer of cyanamide. This result seems only seemingly insignificant, but it shows possible mechanism of guanylation by PyCA which is important step in synthesis of some biological active compounds including antiviral drugs.

Acknowledgments Calculations have been carried out in Wroclaw Centre for Networking and Supercomputing, (http://www.wcss.pl).

Funding The study was financially supported by the ILT&SR PAS statutory activity subsidy, grant no. 2019/5.

Compliance with ethical standards

Conflict of interest The authors declare that they have no conflict of interest.

References

1. Bernatowicz MS, Youling W, Matsueda GR (1992) 1H-Pyrazole-1-carboxamidine hydrochloride: an attractive reagent for guanylation of amines and its application to peptide synthesis. J Organomet Chem 57:2497–2502. https://doi.org/10.1021/jo00034a059
2. Magano J (2009) Synthetic approaches to the neuraminidase inhibitors zanamivir (Relenza) and oseltamivir phosphate (Tamiflu) for the treatment of influenza. Chem Rev 109:4398–4438. https://doi.org/10.1021/cr800449m
3. Kühl N, Graf D, Bock J et al (2020) A new class of dengue and West Nile virus protease inhibitors with submicromolar activity in reporter gene DENV-2 protease and viral replication assays. J Med Chem 63:8179–8197. https://doi.org/10.1021/acs.jmedchem.0c00413
4. Bruno IJ, Cole JC, Edgington PR et al (2002) New software for searching the Cambridge Structural Database and visualizing crystal structures. Acta Crystallogr Sect B Struct Sci 58:389–397. https://doi.org/10.1107/S0108768102003324
5. Groom CR, Bruno IJ, Lightfoot MP, Ward SC (2016) The Cambridge structural database. Acta Crystallogr Sect B Struct Sci Cryst Eng Mater 72:171–179. https://doi.org/10.1107/S2052520616003954
6. Etter MC (1990) Encoding and decoding hydrogen-bond patterns of organic compounds. Acc Chem Res 23:120–126. https://doi.org/10.1021/ar00172a005
7. Daszkiewicz M (2012) Complex hydrogen bonding patterns in bis(2-aminopyrimidinium) selenate monohydrate. Interrelation among graph-set descriptors. Struct Chem 23:307–313. https://doi.org/10.1007/s11224-011-9872-2
8. Sheldrick GM (2008) A short history of SHELX. Acta Crystallogr Sect A Found Crystallogr 64:112–122
9. Sheldrick GM (2015) Crystal structure refinement with SHELXL. Acta Crystallogr Sect C Struct Chem 71:3–8. https://doi.org/10.1107/S2053229614024218
10. Brandenburg K, Putz H (2008) Diamond: crystal and molecular structure visualization. Cryst Impact Bonn, Ger
11. Frisch, M. J., Trucks, G. W., Schlegel, H. B., Scuseria, G. E., Robb, M. A., Cheeseman, J. R., Scalmani, G., Barone, V., Petersson GA (2016) Gaussian 16, Rev. C.01. Gaussian, Inc.

12. Becke AD (1993) Density-functional thermochemistry. III. The role of exact exchange. J Chem Phys 98:5648–5652. https://doi.org/10.1063/1.464913
13. Lee C, Yang W, Parr RG (1988) Development of the Colle-Salvetti correlation-energy formula into a functional of the electron density. Phys Rev B 37:785–789. https://doi.org/10.1103/PhysRevB.37.785
14. Miehlich B, Savin A, Stoll H, Preuss H (1989) Results obtained with the correlation energy density functionals of becke and Lee, Yang and Parr. Chem Phys Lett 157:200–206. https://doi.org/10.1016/0009-2614(89)87234-3
15. Vosko SH, Wilk L, Nusair M (1980) Accurate spin-dependent electron liquid correlation energies for local spin density calculations: a critical analysis. Can J Phys 58:1200–1211. https://doi.org/10.1139/p80-159
16. Grimme S, Ehrlich S, Goerigk L (2011) Effect of the damping function in dispersion corrected density functional theory. J Comput Chem 32:1456–1465. https://doi.org/10.1002/jcc.21759
17. Alcolea Palafox M (2000) Scaling factors for the prediction of vibrational spectra. I. Benzene molecule. Int J Quantum Chem 77:661–684. https://doi.org/10.1002/(SICI)1097-461X(2000)77:3<661::AID-QUA7>3.0.CO;2-J
18. Novak A (1979) Vibrational spectroscopy of hydrogen bonded systems. Infrared and Raman spectroscopy of biological molecules, In, pp 279–303